ARMY RESEARCH LABORATORY

Onset and Nature of Fracture of Uniaxially Compressed Gun Propellants

A Small Angle Neutron and X-ray Scattering Study

Robert J. Lieb
Samuel F. Trevino
John D. Barnes

ARL-TR-185 August 1993

NOTICES

Destroy this report when it is no longer needed. DO NOT return it to the originator.

Additional copies of this report may be obtained from the National Technical Information Service, U.S. Department of Commerce, 5285 Port Royal Road, Springfield, VA 22161.

The findings of this report are not to be construed as an official Department of the Army position, unless so designated by other authorized documents.

The use of trade names or manufacturers' names in this report does not constitute indorsement of any commercial product.

REPORT DOCUMENTATION PAGE

Form Approved
OMB No. 0704-0188

1. AGENCY USE ONLY *(Leave blank)*	2. REPORT DATE	3. REPORT TYPE AND DATES COVERED
	August 1993	Final Oct 1991 - May 1993

4. TITLE AND SUBTITLE

Onset and Nature of Fracture of Uniaxially Compressed Gun Propellants - A Small Angle Neutron and X-ray Scattering Study

5. FUNDING NUMBERS

PR: 1L161102AH43

6. AUTHOR(S)

Robert J. Lieb, Samuel F. Trevino and John D. Barnes

7. PERFORMING ORGANIZATION NAME(S) AND ADDRESS(ES)

US Army Research Laboratory
ATTN: AMSRL-WT-PE
Aberdeen Proving Ground, MD 21005-5066

8. PERFORMING ORGANIZATION REPORT NUMBER

9. SPONSORING/MONITORING AGENCY NAMES(S) AND ADDRESS(ES)

US Army Research Laboratory
ATTN: AMSRL-OP-CI-B (Tech Lib)
Aberdeen Proving Ground, MD 21005-5066

10.SPONSORING/MONITORING AGENCY REPORT NUMBER

ARL-TR-185

11. SUPPLEMENTARY NOTES

12a. DISTRIBUTION/AVAILABILITY STATEMENT

Approved for public release; distribution is unlimited.

12b. DISTRIBUTION CODE

13. ABSTRACT *(Maximum 200 words)*

To understand the mechanism of fracture, the response of two propellant formulations, M30 and M43, has been studied. Specimens were prepared from extruded solid strands and uniaxially deformed at about 100 1/s to 2, 5, 10 and 20 percent strain. Axial and ortho-axial sections of these damaged specimens were investigated with small angle neutron and X-ray scattering. Monochromatic beams irradiated the specimens and the resulting scattering patterns were recorded as a function of scattering angle with a two-dimensional detector. These measurements were performed using instruments at the National Institute of Standards and Technology (NIST). The scattering from both propellants showed substantial asymmetry and dramatic changes as a function of strain. These results directly reflect the surface area that exists between regions of different materials and also any new surface area created by fracture. Interpretation of the measurements has for the first time revealed important aspects of the mechanism of fracture failure in these propellants.

14. SUBJECT TERMS

mechanical response; propellants; bed; M30; M43; x rays; surface profile; fracture damage; scattering; neutrons; small angle; x ray scattering

15. NUMBER OF PAGES

28

16. PRICE CODE

17. SECURITY CLASSIFICATION OF REPORT	18. SECURITY CLASSIFICATION OF THIS PAGE	19. SECURITY CLASSIFICATION OF ABSTRACT	20. LIMITATION OF ABSTRACT
UNCLASSIFIED	UNCLASSIFIED	UNCLASSIFIED	SAR

Intentionally Left Blank

TABLE OF CONTENTS

Intentionally Left Blank

LIST OF FIGURES

Intentionally Left Blank

ACKNOWLEDGMENTS

We would like to thank M. G. Leadore of the Army Research Laboratory for preparing and compressing the specimens, C. S. Choi of the National Institute of Standards and Technology (NIST) for assistance in obtaining the diffraction pole figures, J. Barkley (NIST) for valuable suggestions with reference to the neutron small angle scattering, and G. Long and S. Kreuger (NIST) for help in the absolute calibration of the X-ray scattering.

Intentionally Left Blank

1. INTRODUCTION

Pressure generation within guns is known to depend on the amount of surface area of the propelling charge. Generation of fracture surface area can occur when mechanical loads are applied to the propellant grains during ignition and combustion. Many studies[1-6] have been undertaken to establish the link between the mechanical response to deformation and the surface area generation that results from mechanical damage. Results of these studies have led to improvements in performance and propellant vulnerability responses, but have not revealed the nature of fracture onset and growth within the propellant.

The measurement of surface area created by mechanical damage has been performed in various ways. Pycnometery and the closed bomb burning of damaged specimens have been used and they offer insight into the extent of fracture damage of propellant specimens. However, in order for the results to be optimally used, the experimental results must be related to the influence that the damage has on propellant combustion. Problems occur when the results are interpreted. For example, the surface area measured by the pycnometer may not be accessible to the flame, or, conversely, the flame may avail itself to much more area than the pycnometer can measure. Closed bomb analysis seems to provide the most direct measurement, but, even there, dynamic effects, such as the ease of the ignitibiliy of freshly fractured surfaces or the nature of fracture surface area generation under the influence of the dynamic environment, raise questions about applicability of the experimental results to the operational environment situation. It is imperative, therefore, that as much as possible be known about the fracture process, including its onset and early development so that the applicability of test methods and results can be properly made. One method that can be used to investigate the boundary surfaces of a system is to scatter radiation from the system and to analyze the results.

Neutron and x-ray scattering by a specimen depend on contrast modulation throughout the specimen. These modulations can be caused by a change in density, or scattering cross section. For the radiation used in the present, the interface boundaries are probed. In a homogeneous material, fracture will increase the scattering cross section by introducing the fracture surface. In a composite consisting of materials of different contrast, scattering will occur at the interface boundaries. This scattering will be increased by fracture occurring either by separation of the component materials or by bulk fracture.

These scattering features offer a method by which the onset and nature of the fracture process can be investigated. Since the greatest change in scattering attributable to fracture would be expected to occur in composite materials, composite propellants, M30 (Lot RAD-PE-753-12B) and M43 (Lot

IH90L-E-00025), were selected for this investigation. Specimens were prepared and uniaxially compressed at a high rate of deformation to various strain levels that ranged from 0% to 20%. The changes in the structure of these materials caused by this treatment were investigated by small angle scattering of both neutrons and x-rays. These measurements revealed the onset and nature of growth of the damage. This information offers significant insight into the fracture process and helps direct future research efforts aimed at uncovering important processes that occur during propellant combustion.

The experimental methods used here will clearly apply to the study of a large range of composite material studies.

2. NEUTRON AND X-RAY SMALL ANGLE SCATTERING

The theory and practice of scattering of neutrons and x-rays are well established[7]. Improvements in the instrumentation and adaptations of the theory to understand the physics in new materials continue. Here, we focus on those aspects that address the present work.

Both types of radiation are able to scatter coherently from centers of which the material is composed. For neutrons, these scattering centers are the nuclei and for x-rays, they are the electrons of the atoms in the material. Since the scattering is coherent, it carries information about the geometric properties of the conglomerate of scattering centers. An essential quantity that describes the radiation is the wave vector **Q** whose magnitude is given by

$$Q = \frac{4\pi}{\lambda} \sin\theta, \tag{1}$$

where λ is the wavelength of the radiation and 2θ is the scattering angle. The scale, r_s, of the geometry to which the radiation is sensitive is of order

$$r_s = \frac{2\pi}{Q} \tag{2}$$

Typical values of the radiation wavelength range from 0.1 to 1 nm (1 to 10 Å) so that the study of structures with geometric scales of 100 nm requires scattering angles of about 1° or less (thus small angle scattering). The structures of this scale size will reveal themselves if contrast modulations scatter the probe radiation. The specimen may consist of different materials or a material and voids. The scattering length density, ρ_i, for material *i* can be calculated from measured properties of the scattering centers of which it is composed, and is given by

$$\rho_i = \frac{N_A D_i \sum_k n_k b_k}{\sum_k W_k} \qquad (3)$$

where N_A is the Avogadro constant, D_i is the mass density of material *i*, the sums are over the *k* atom types in material *i*, n_k is the number of atoms of type *k*, W_k is the atomic weight of atom type *k*, and b_k is the scattering length of atom type *k* for the radiation of wavelength λ. Note that the dimension of ρ is L^{-2}. For neutrons, the values of b_k for the various materials are available as measured quantities, whereas for x-rays, $b_k = Z_k b_e$, in which Z_k is the atomic number of atom *k* and b_e is the scattering length of a single electron for x-rays, namely, the classical electron radius. These quantities are listed in Table 1 and are based on the formulas for M30 and M43, also provided in the table. The only requirement for coherent scattering to occur is that $(\Delta\rho_{ij})^2$ between the two materials *i* and *j* be non-zero. Note that ρ_i of material *i* is different for neutrons and x-rays, but of more importance is that the contrast of materials *i* and *j* is also different for neutrons and x-rays. This last observation is particularly useful when the system being studied consists of three components (as is the case here).

The dependence of the scattering intensity I(Q) on Q is different for different magnitudes of Q even for the same material. This can be understood from Equation 2. The region of interest in the present work is known as Porod[7] scattering and is valid for the range of Q sensitive to the surface area of the geometric structure. In this region the intensity is given as

$$I(Q) = 2\pi \frac{\sum_{ij} (\Delta\rho_{ij})^2 S_{ij}}{Q^4}, \qquad (4)$$

where the sum is over pairs of materials *ij* between which there exists a boundary of *specific* surface S_{ij}, i.e., surface area per unit volume of sample. In the present work, the propellants consist of three materials, the filler, F, the binder, B, and voids, V. There are, therefore, three specific surface areas to be determined S_{FB}, S_{FV} and S_{BV}. Only two measurements are available, namely, I_n and I_x, the neutron and x-ray intensities. As indicated above, voids can exist in the binder, filler, or between binder and filler. If these voids had been accessible to the outside, they could have been filled with a contrasting liquid making available another set of independent data. This was attempted without

Table 1. Neutron and X-ray Scattering Length Density for the Composite Propellant Filler and Binder

Compnoent	Weight Percent	Volume Percent	ΣW (g/mole)	D (g/cc)	ΣZ	ρ_n (10^9 cm^{-2})	$\rho_{X\text{-ray}}$ (10^9 cm^{-2})
M30							
NQ (filler)	48	46.3	104	1.81	54	42.5	159
NC (binder)	28	29.5	272	1.655	140	33.8	144
NG (binder)	22	24.1	227	1.591	116	34.6	138

Net Filler & Binder Scattering Length Density

$\rho_{F_n} = 42.5 \times 10^9$ cm^{-2} $\quad \rho_{F_{X\text{-ray}}} = 159 \times 10^9$ cm^{-2}

$\rho_{B_n} = 34.2 \times 10^9$ cm^{-2} $\quad \rho_{B_{X\text{-ray}}} = 141 \times 10^9$ cm^{-2}

M43								
RDX	(filler)	76	69.3	222	1.80	114	43.8	159
NC	(binder)	4	4.0	272	1.655	140	33.7	144
CAB	(binder)	12	17.2	330	1.16	176	13.6	105
Plast.	(binder)	8	9.5	320	1.39	166	25.4	122

Net Filler & Binder Scattering Length Density

$\rho_{F_n} = 43.8 \times 10^9$ cm^{-2} $\quad \rho_{F_{X\text{-ray}}} = 159 \times 10^9$ cm^{-2}

$\rho_{B_n} = 21.1 \times 10^9$ cm^{-2} $\quad \rho_{B_{X\text{-ray}}} = 117 \times 10^9$ cm^{-2}

b_k & b_e Values

Element	b_k (10^{-12} cm)
C	0.6648
H	-0.3741
N	0.930
O	0.5805

$b_e = 0.28 \times 10^{-12}$ cm

success as a part of this investigation. Therefore, a simple model is used here in which each void presents an equal surface to each of the filler and binder materials. During propellant manufacture, the filler is wetted by the binder and extruded. Voids *within* the binder or filler alone comprise a very small amount of the interface surface. It is thought that any new fracture surface would occur *between* the binder and filler, as is usually seen in micrographs of these materials after fracture damage has occurred. These observations help justify considering this model, in which $S_{FV} = S_{BV} = \frac{1}{2} S_1$. Using this assumption, the two measurements of the neutron and x-ray intensities yield the equation

$$I_m = 2\pi \frac{\left[(\rho_{F_m}^2 + \rho_{B_m}^2) \frac{S_1}{2} + (\rho_{F_m} - \rho_{B_m})^2 S_{FB} \right]}{Q^4} \tag{5}$$

where *m* represents the radiation type, either neutrons or x-ray. Inversion of these equations yields a direct measure of the two specific surfaces.

3. EXPERIMENTAL PROCEDURE

3.1 Preparation of Propellant Specimens The specimens were prepared by cutting extruded solid sticks of propellant into right circular cylinders (diameter = 12.7 mm) with a length of 10.0 mm using a diamond saw. Two sets of five specimens were prepared for each propellant, and each set was uniaxially strained to 0% (undamaged), 2%, 5%, 10% and 20%. The compression was conducted in a servohydraulic test fixture, illustrated in Figure 1. The unique feature about this machine is that compression can be arrested at a selected strain by adjusting the height of the anvil. As the actuator moves down, the force gauge comes into contact with the specimen and compression begins. It is halted when the inside surface of the impact bell contacts the mated surface of the impact cone. The nitrogen cylinder then absorbs the residual system energy by moving the piston. Therefore, the level of strain can be selected by adjusting the anvil height. The compressive strain rate was 100 s^{-1}.

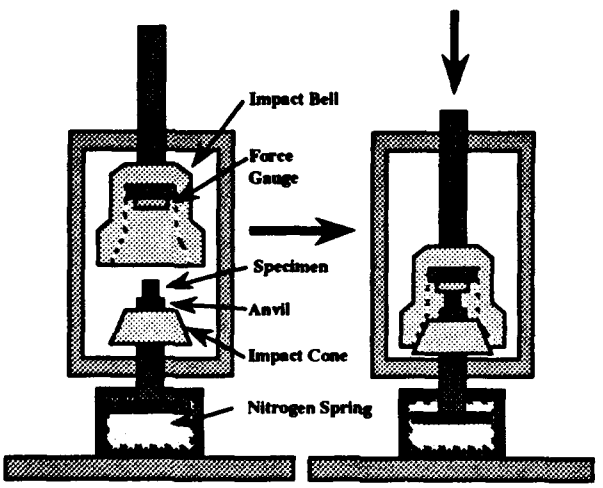

Figure 1. Servohydraulic Tester

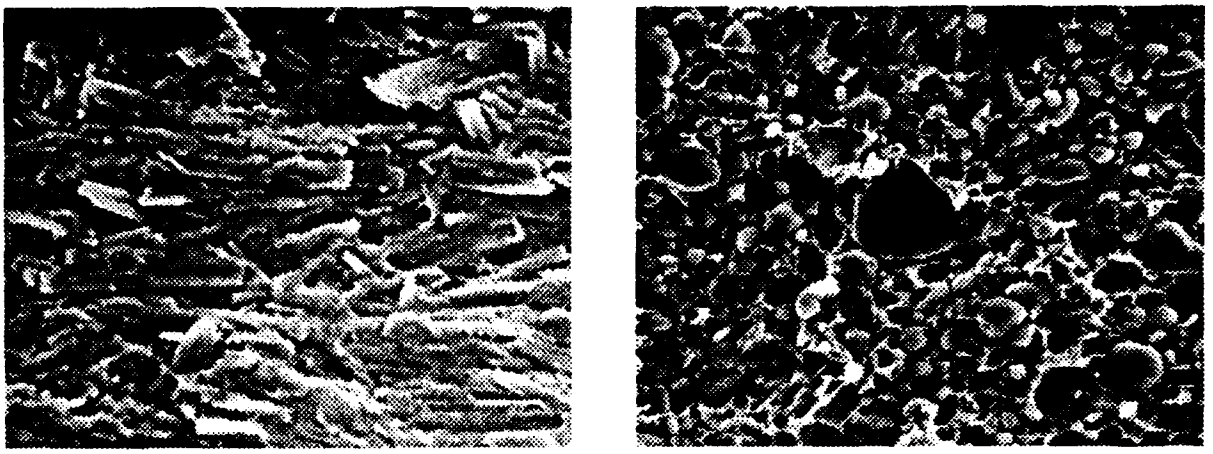

Figure 2. SEM Micrographs of the Propellant Specimens

The filler in M30 is nitroguanidine (NQ), which is in the form of long, needle-like crystals of diameter from 5 to 10 μm. The nitrocellulose (NC) and nitroglycerin (NG) form an intimate mixture (solution) which acts as a binder for the system. The filler in M43 is cyclotrimethylene-trinitramine (RDX) and is of significantly different form than the filler in the M30 system. The RDX is ground into small (1 to 20 μm) ellipsoidal crystals that are held together by the intimately mixed cellulose acetate butyrate (CAB)/NC/plasticizer binder. The adhesive binding strength in this system is much weaker than that of the M30 system. Figure 2 shows scanning electron micrographs of split propellant specimens that reveal the undamaged, intrinsic, propellant morphology.

After compression, the propellant cylinders were cut into 1-mm-thick scattering specimens, as illustrated in Figure 3. Two types of specimens were made. Type A was cut perpendicular to the cylinder axis and Type B was cut parallel to the axis and through the center of the cylinder. The two types were needed to detect in greater detail the way in which damage occurs. Note that the alignment of the NQ, which occurs during the extrusion process, is along the axis of the grain, as shown in Figure 3. This orientation is presented differently to the beams in the Type A and Type B specimens (hereafter simply referred to as A or B), as shown in Figure 4.

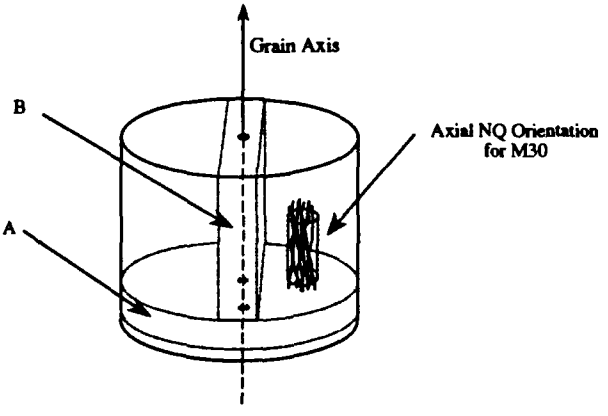

Figure 3. Illustration of Type A and B Specimens

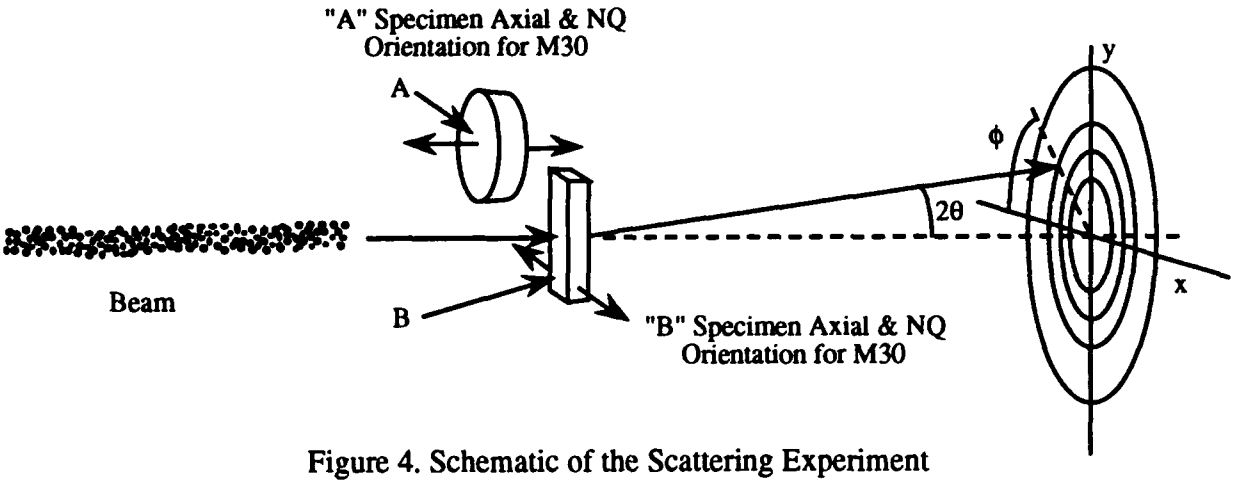

Figure 4. Schematic of the Scattering Experiment

3.2 Scattering Measurements Both the neutron and x-ray spectrometers are located at the National Institute for Standards and Technology (NIST). Figure 4 is a schematic appropriate for both instruments. The method of obtaining the monochromatic beam of radiation differs for each technique, but the subsequent characteristics are essentially the same. The neutron beam wavelength was 8 Å (v_n = 490 m/s) and the x-ray wavelength was 1.5 Å (Cu Kα). The direction of the neutron beam is defined by two circular slits separated by distances of the order of 1 m. The distance between the sample and detector is about 8 m. These two geometries determine the angular resolution of the instrument. The detector is a two-dimensional, position-sensitive device that collects data simultaneously in a plane perpendicular to the incident beam. The data are stored in digital form for subsequent analysis. This includes the ability to obtain averages for constant scattering angle (θ) as functions of the azimuthal angle (ϕ). If radial asymmetry exists in the scattering pattern, sector averages for azimuthal angles are readily performed. The data-collection time for the present set of measurements totalled approximately 6 hours for each specimen.

4. RESULTS

The neutron and x-ray scattering patterns for each specimen were qualitatively similar. Different amounts of radial asymmetry were obtained for the different degrees of strain. The B specimen of unstrained M30 produced the greatest degree of asymmetry. A plot of the raw, two-dimensional data is presented in Figure 5. The asymmetry is attributable to the orientation of the NQ needle-like crystal along the specimen axis. For all the B specimen data, 30°-sector averages centered about ϕ were performed, with ϕ equal to 0°, 30°, 60°, and 90°. The data were corrected for detector efficiency and for background and were normalized to standard samples from which absolute cross sections are determined. Sector averages were not performed for the A specimens because they showed radially

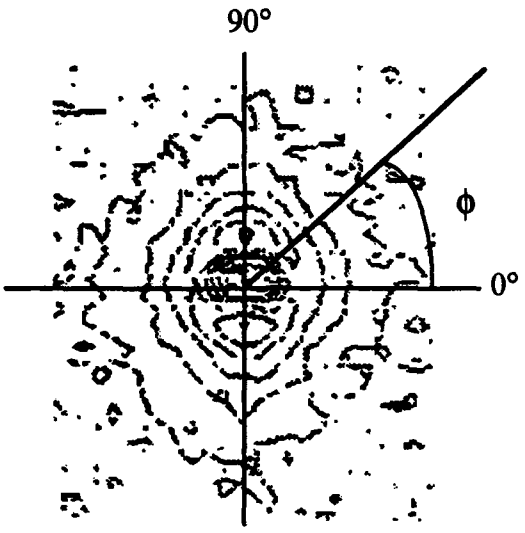

Figure 5. Undamaged B Type Scattering Results for M30 Showing NQ Alignment

symmetric scattering. The coefficient of Q^{-4}, which is associated with the contrast and specific surface factor in Equation 5, is obtained by plotting IQ^4 vs Q^4, fitting a straight line for the appropriately chosen values of Q, and determining the intercept. This was done for both neutron and x-ray data. Equation 5 was inverted to obtain S_1 and S_{BF}. Figures 6 and 7 present the values of these specific surface areas for both propellants as functions of strain for the A and B specimens, and for sector averages for B specimens. For the B specimens, ϕ equal to 0° corresponds to the axial direction of the specimen. Note that there should be good agreement between the scattering produced by the undamaged A specimens and the undamaged B specimens at ϕ equal to 90°, since these directions are the same. This agreement should extend to the damaged specimens as long as nature and degree of damage remain the same in both specimens.

5. ANALYSIS

5.1 M30 Figure 6 shows the specific area S_1 and S_{FB} plotted against strain and axial orientation. The specific area is the interface area per unit volume of material and is given in units of cm^{-1}. S_1 values for the specimens indicate that very few voids were present in the undamaged material. Previous M30 propellant micrographs indicated that there were no voids in the binder. However, crystalline NQ from another investigation, shown in Figure 8, reveals voids on the surface of the NQ crystals. This micrograph and others from this series indicate that hollow NQ crystals could result from these elongated voids being internalized and could account for the low but nonzero initial S_1 values. The match in the S_1 values for the A specimen and the B specimen at ϕ equal to 90° is demonstrated for the undamaged specimens, and the damage trends followed each other, but the B specimen showed significantly more separation at 5% strain.

As strain increased, the A specimen showed an increase in S_1 until 5% strain, after which S_1 leveled off and then increased again at higher strain. This is consistent with separation of binder and filler with the internal voids of the NQ staying unchanged. The B specimens followed the same trend as the A specimen with generally more separation observed at larger angles. This indicated that

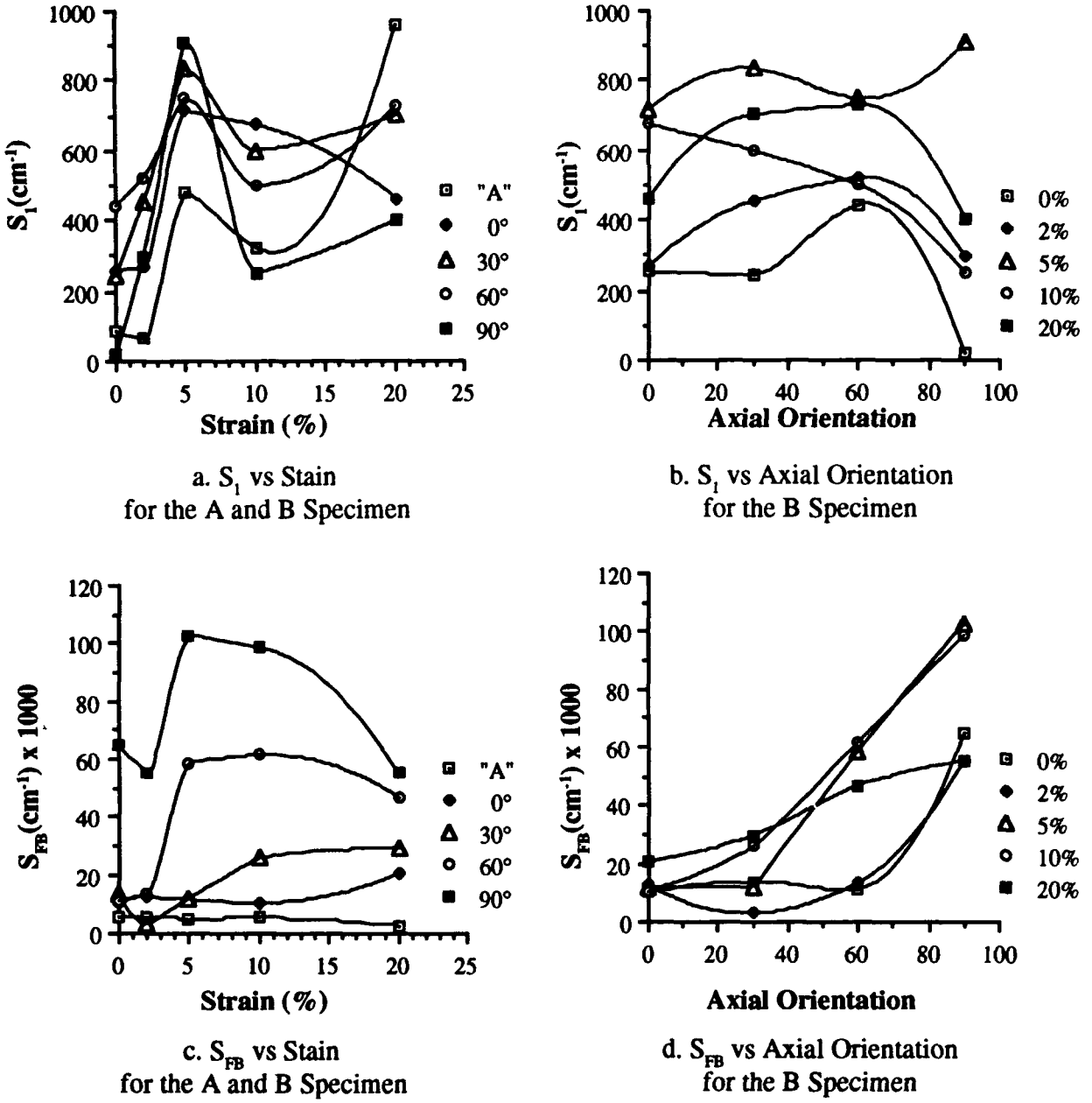

a. S_1 vs Stain
for the A and B Specimen

b. S_1 vs Axial Orientation
for the B Specimen

c. S_{FB} vs Stain
for the A and B Specimen

d. S_{FB} vs Axial Orientation
for the B Specimen

Figure 6. Specific Surface Area for M30 Propellant

separation occurred at the binder-filler interface, since more surface is exposed at greater angles because of the NQ alignment in the axial direction. The generally lower values for the A specimen indicate that less damage was produced at the specimen ends than in the middle. The rapid drop in S_1 after 5% strain indicated that some closing of the newly created surfaces occurred as the NQ crystals began to reorient (bend). At 20% strain, the values of S_1 showed a loss of the previously mentioned order with angle, indicating a more random reorientation of the NQ crystals as they continue to bend and break.

In Figure 6b the S_1 values for the B specimen are plotted against axial orientation with strain level for each curve remaining constant. The general trend indicated is an increase in S_1 to 5% strain, then a slight reduction as some surfaces recombine at 10%, and an increase again at 20% with some surface reorientation. Note that for the undamaged specimen, the S_1 values remain about constant as ϕ increases, and that the creation of new S_1 surface in the damaged specimens tended to increase with ϕ until recombination and reorientation occurred at the higher strain. Note that the information in Figures 6a and 6b (as in 6c and 6d) is the same but presented from a different perspective.

In Figure 6c, the S_{FB} values are plotted in a manner similar to the values in Figure 6a. The change in magnitude between the S_1 and S_{FB} values reflects the much larger surface that exists between binder and filler than occurs with voids. The S_{FB} values at zero strain show a good match between the A specimen and B specimen at ϕ equal to 90°. The values were very low along the 0° and 30° direction, as they should be with little surface between binder and filler in this direction. The rise in values with increasing strain for these low angles may be attributed to the reorientation of NQ crystals. The perplexing feature of this plot is the enormous increase in S_{FB} at 60° and 90° at 5% strain. A mechanism accounting for this increase could be the precipitation of NG, which is a liquid, from the binder mixture. This would create new binder-filler surface and still allow separation surfaces to be created. The decrease of S_{FB} at higher strains is in line with continued separation, and the magnitudes need not be reflected in corresponding increases of S_1.

The changes in values of S_{FB} with axial orientation are shown in Figure 6d and follow what was expected at each strain level. All values were low in the ϕ equals 0° direction (axial direction) and increase as ϕ increases. This was expected and reflected the alignment of the NQ crystals. However, the unexpected increase in S_{FB} with strain is again clearly displayed.

5.2 M43 The specific area values for M43 are displayed in Figure 7. This propellant showed no voids in the undamaged specimens. In the B specimen, S_1 showed increasing values at increasing strains, and generally higher values in damaged specimens at increasing ϕ values. This indicated separation of the binder-filler interface, since the binder deforms plastically at 20°C and no fractured RDX has been observed in micrographs of grains damaged during these conditions. Two features in the S_1 curves need to be commented upon. The first concerns the divergence of the S_1 values for the A specimen and the B specimen for ϕ equals 90° at increasing strain. These values should track with each other because the surface area created here is the result of binder-filler separation, and axial alignment is much reduced from that in the M30 propellant. These data suggested a significant difference in the degree of damage in the two scattering specimens, which was subsequently verified.

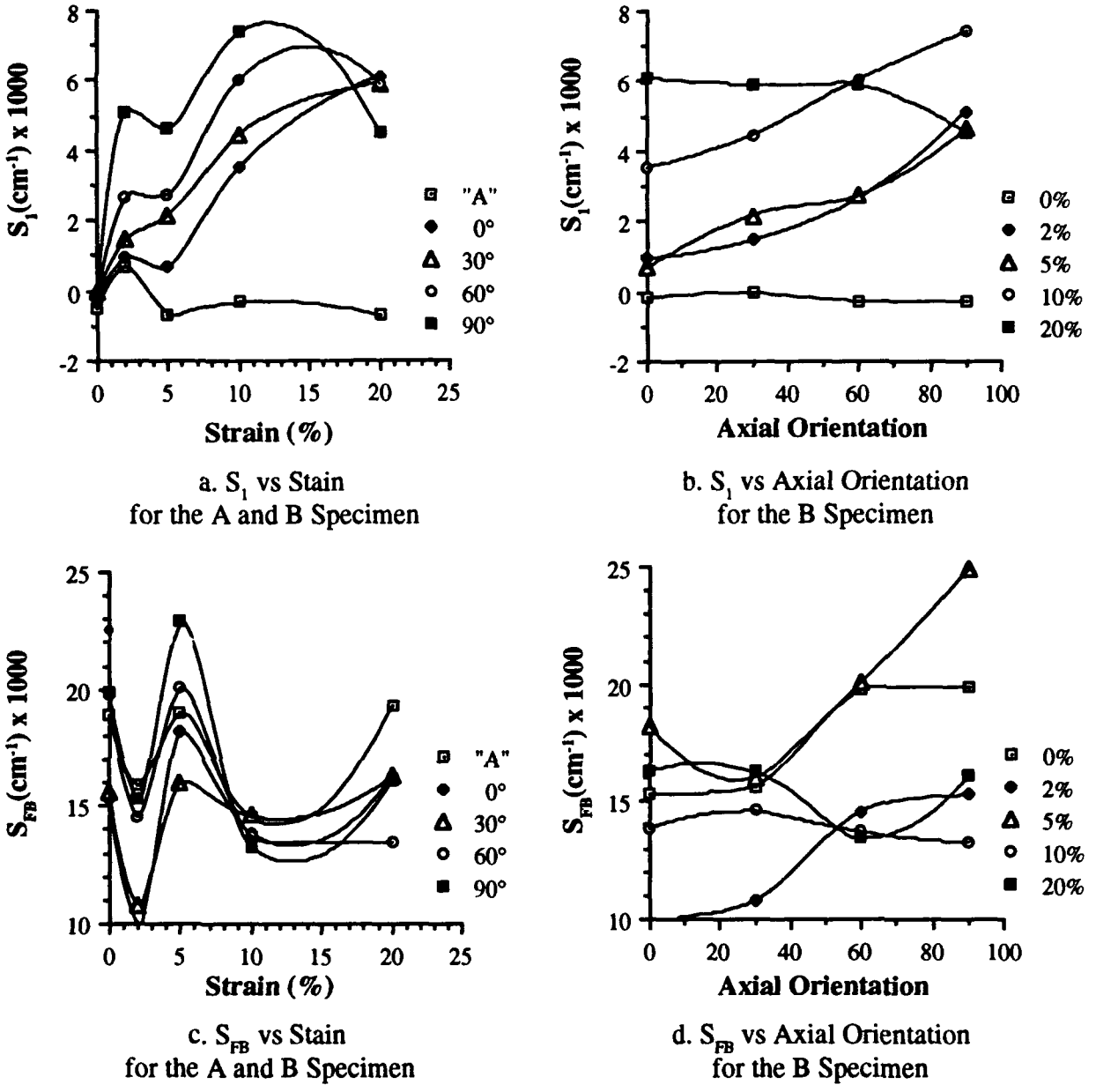

a. S_1 vs Stain for the A and B Specimen

b. S_1 vs Axial Orientation for the B Specimen

c. S_{FB} vs Stain for the A and B Specimen

d. S_{FB} vs Axial Orientation for the B Specimen

Figure 7. Specific Surface Area for M43 Propellant

The mechanism of failure is by shear along 45° cones, as illustrated in Figure 9. Since the A specimen was taken from the end of the uniaxial compression specimen, the A specimen had areas of failure in a ring near the circumference leaving the center relatively damage free. The B specimen, on the other hand, contains the central portion of the compressed specimen, at which the 45° failure cone is directed. Thus, the B specimens contained greater amounts of damaged material, as observed. The second feature concerns the change in S_1 values with axial orientation (see Figure 7b). The increase in S_1 as ϕ increases shows that binder-filler separation preferentially occurred on the lateral surfaces

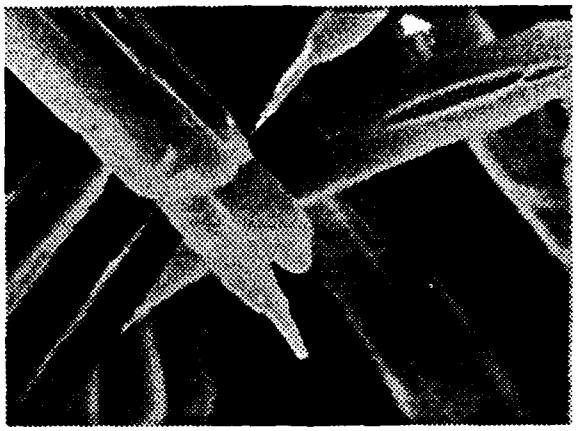

Figure 8. Micrograph of NQ Crystals Showing Surface Voids

Figure 9. Type B Specimen at 20% Strain Showing 45° Failure Surfaces

of the crystal to as much as 10% strain. At 20% strain this trend with ϕ changes indicating that the RDX crystals suffering interface damage were becoming so loose within the matrix that they were able to rotate. This would cause what was observed, a more rapid increase in S_1 at lower ϕ values and reduction in S_1 at higher ϕ values.

The S_{FB} curves plotted against strain show rapidly decreasing surface area immediately upon deformation, rejoining or reforming of the separated surfaces at about 5% strain, and then another significant separation occurring at 10% strain with the net separation remaining about the same through 20% strain. Note that the A specimen and the B specimen at ϕ equal to 90° matched well, as expected, and the A specimen again showed significantly less damage. The changes in S_{FB} with axial orientation showed these same features and made another observation clear, as well. The ellipsoidal shapes of the RDX crystals appeared to align with the axial direction of the specimen. This was indicated by the increasing values of S_{FB} at increasing ϕ for the undamaged, 2%, and 5% strain specimens (see Figure 7d). At the higher strains, the onset of rotation of the crystals noted above disrupts this trend. These observations provide a consistent picture and add significant insight into the failure process for M43 propellant.

One additional piece of information that adds credence to the interpretation of these measurements is given in a recent determination of the surface area per gram of RDX crystals[9], which was made before mixing the crystals with the binder. The value of the surface area density, S_d, was found to be 1.86×10^4 cm^2/g. This can be converted to specific density for M43 by using

$$S_{FB} = S_d \, \delta_F \, v_F, \tag{6}$$

in which δ_F and v_F are the mass density and volume fraction of the filler in the M43, respectively. The density of RDX is 1.80 g/cm^3 and its volume fraction in M43 propellant is 0.675. When these values are used, the specific surface value received is 2.26×10^4 cm^{-1}. This value is in good agreement with the values measured here for the undamaged specimens. (See Figure 7c, where the dot on the y-axis shows this value.)

6. CONCLUSIONS

A new method has been found for investigating the changes in surface morphology of filled energetic materials. Neutron and x-ray scattering were used to measure the binder-filler and void surfaces in M30 and M43 gun propellant as a function of strain and axial asymmetry of the specimen.

For the M30 propellant, scattering measurements showed many features of the propellant system, including previously noted axial alignment of the NQ crystals; the large binder-filler surface area orthogonal to the crystal axis; the strain level at which fracture begins; and the nature of the failure mechanism, that is, binder-filler separation. Also indicated in the data was the relatively small level of specific surface area attributed to voids, rejoining of separated portions of damaged propellant after a certain strain level, and the reorientation of NQ crystals at high strain. One result that is not well understood was the indication of dramatic increases in binder-filler surface area. This was unexpected and may be attributable to an occurrence such as the precipitation of nitroglycerin (a liquid) from the binder mixture. Efforts to understand these results are continuing.

It seems that for M30, there was little free surface area (S_1) and not much new separation area created in the early deformation. Between 2% and 5% strain, most of the separation damage was created, and at larger strains, some reconnection of separated surfaces occurred. At even greater strain, no significant increase occurred, as if the additional strain only deformed the already separated surfaces by bending. The evolution of the binder-filler interface surface (S_{FB}) in M30 shows a modest reduction at low strain and then underwent some unanticipated mechanism (as mentioned above) that created more binder-filler surface.

The most significant morphological features observed for M43 propellant were absence of voids before compression, and the axial alignment of the major axis of the ellipsoidal RDX particles along the specimen axis. This alignment was much less than that for M30 but still observable. Upon compression, the degree of damage was much less in the A specimen because of the shear failure occurring in the specimen and the method of specimen preparation, explained above.

Results suggested that when deformation occurred in M43, binder-filler separation began immediately and increased steadily throughout the deformation. Some recombination of separated interface of binder-filler surface seems to occur at about 5% strain. However, as compaction continued the separation grew, and there was an indication that RDX crystals became free to rotate in the matrix somewhere between 10% and 20% strain.

This information was largely unknown before these experiments were performed. These new insights will help guide the development of propellants and will aid in the development of methods for increased performance and reduced vulnerability response.

The scattering techniques that were developed in these studies will permit more extensive progress in future scattering efforts. Low temperature deformation will be investigated to further study the onset of fracture with a more brittle binder. Other experiments on single- and double-base propellants will offer similar insight into the fracture mechanisms of unfilled propellant systems and will provide methods for improving the understanding of the failure process.

It is clear, from the successful application of both neutron and x-ray scattering in the present study, that this method of obtaining information about the microstructure of composite materials has wide application. This is especially important in situations when voids in the material are not accessible and when the condition of the interface between material components is of some consequence to the properties of the composite. Manufacturing processes such as pelletting, in which parameters such as strain rate and temperature can be controlled, would probably benefit greatly by the use of these methods to characterize the state of the material.

7. REFERENCES

1. Gazonas, G. A., A. Juhasz, and J. C. Ford, "Strain Rate Insensitivity of Damaged-Induced Surface Area in M30 and JA2 Gun Propellants," BRL-TR-3251, USA Ballistic Research Laboratory, Aberdeen Proving Ground, MD, August 1991.

2. Lu, P., B. Strauss, S. Moy, and R. Lieb. "Shaped Charge Jet Impact on Gun Propellants Study I - Temperature and Mechanical Properties Effects," 1991 Propulsion System Hazards Subcommittee Meeting, March 1991.

3. Lieb, R. J., and M. G. Leadore, Mechanical Failure Parameters in Gun Propellants," BRL-TR-3296, USA Ballistic Research Laboratory, Aberdeen Proving Ground, MD, November 1991.

4. Gazonas, G.A., "The Mechanical Response of M30, XM39, and JA2 Propellants at Strain Rates from 10^{-2} to 250 sec^{-1}." BRL-TR-3181, USA Ballistic Research Laboratory, Aberdeen Proving Ground, MD, January 1991.

5. Lieb, R. J., and M. G. Leadore, "Mechanical Response of Gun Propellant Beds at Low Strain Rates," ARL-TR-78, US Army Research Laboratory, Aberdeen Proving Ground, MD, February, 1993.

6. Horst, A.W., "The role of Propellant Mechanical Properties in Propelling Charge Phenomenology," 1981 JANNAF Structures and Mechanical Behavior Subcommittee Meeting, 1, CPIA Publication 351, December 1981.

7. Glatter, O. and O. Kratky, Ed., *Small Angle X-ray Scattering*, Academic Press, NY, 1982.

8. Simmons, R., Private Communication, Naval Surface Warfare Center, Indian Head, MD, 1992.

9. Caulder, S., Private Communication, Naval Surface Warfare Center, Indian Head, MD, 1992.

Intentionally Left Blank

No. of Copies	Organization
2	Administrator Defense Technical Info Center ATTN: DTIC-DDA Cameron Station Alexandria, VA 22304-6145
1	Commander U.S. Army Materiel Command ATTN: AMCAM 5001 Eisenhower Ave. Alexandria, VA 22333-0001
1	Director U.S. Army Research Laboratory ATTN: AMSRL-OP-CI-AD, Tech Publishing 2800 Powder Mill Rd. Adelphi, MD 20783-1145
1	Director U.S. Army Research Laboratory ATTN: AMSRL-OP-CI-AD, Records Management 2800 Powder Mill Rd. Adelphi, MD 20783-1145
2	Commander U.S. Army Armament Research, Development, and Engineering Center ATTN: SMCAR-IMI-I Picatinny Arsenal, NJ 07806-5000
2	Commander U.S. Army Armament Research, Development, and Engineering Center ATTN: SMCAR-TDC Picatinny Arsenal, NJ 07806-5000
1	Director Benet Weapons Laboratory U.S. Army Armament Research, Development, and Engineering Center ATTN: SMCAR-CCB-TL Watervliet, NY 12189-4050
1	Director U.S. Army Advanced Systems Research and Analysis Office (ATCOM) ATTN: AMSAT-R-NR, M/S 219-1 Ames Research Center Moffett Field, CA 94035-1000

No. of Copies	Organization
1	Commander U.S. Army Missile Command ATTN: AMSMI-RD-CS-R (DOC) Redstone Arsenal, AL 35898-5010
1	Commander U.S. Army Tank-Automotive Command ATTN: AMSTA-JSK (Armor Eng. Br.) Warren, MI 48397-5000
1	Director U.S. Army TRADOC Analysis Command ATTN: ATRC-WSR White Sands Missile Range, NM 88002-5502
(Class. only) 1	Commandant U.S. Army Infantry School ATTN: ATSH-CD (Security Mgr.) Fort Benning, GA 31905-5660
(Unclass. only) 1	Commandant U.S. Army Infantry School ATTN: ATSH-WCB-O Fort Benning, GA 31905-5000
1	WL/MNOI Eglin AFB, FL 32542-5000
	Aberdeen Proving Ground
2	Dir, USAMSAA ATTN: AMXSY-D AMXSY-MP, H. Cohen
1	Cdr, USATECOM ATTN: AMSTE-TC
1	Dir, ERDEC ATTN: SCBRD-RT
1	Cdr, CBDA ATTN: AMSCB-CII
1	Dir, USARL ATTN: AMSRL-SL-I
10	Dir, USARL ATTN: AMSRL-OP-CI-B (Tech Lib)

No. of Copies	Organization
1	Chairman DOD Explosives Safety Board Room 856-C Hoffman Bldg. I 2461 Eisenhower Avenue Alexandria, VA 22331-0600
1	Headquarters U.S. Army Materiel Command ATTN: AMCICP-AD, M. Fisette 5001 Eisenhower Ave. Alexandria, VA 22333-0001
1	U.S. Army Ballistic Missile Defense Systems Command Advanced Technology Center P.O. Box 1500 Huntsville, AL 35807-3801
1	Department of the Army Office of the Product Manager 155mm Howitzer, M109A6, Paladin ATTN: SFAE-AR-HIP-IP, Mr. R. De Kleine Picatinny Arsenal, NJ 07806-5000
3	Project Manager Advanced Field Artillery System ATTN: SFAE-ASM-AF-E, LTC A. Ellis T. Kuriata J. Shields Picatinny Arsenal, NJ 07801-5000
1	Project Manager Advanced Field Artillery System ATTN: SFAE-ASM-AF-Q, W. Warren Picatinny Arsenal, NJ 07801-5000
2	Commander Production Base Modernization Agency U.S. Army Armament Research, Development, and Engineering Center ATTN: AMSMC-PBM, A. Siklosi AMSMC-PBM-E, L. Laibson Picatinny Arsenal, NJ 07806-5000
4	PEO-Armaments Project Manager Tank Main Armament System ATTN: AMCPM-TMA AMCPM-TMA-105 AMCPM-TMA-120 AMCPM-TMA-AS, H. Yuen Picatinny Arsenal, NJ 07806-5000
4	Commander U.S. Army Armament Research, Development, and Engineering Center ATTN: SMCAR-CCH-V, C. Mandala E. Fennell SMCAR-CCH-T, L. Rosendorf SMCAR-CCS Picatinny Arsenal, NJ 07806-5000
19	Commander U.S. Army Armament Research, Development, and Engineering Center ATTN: SMCAR-AEE, J. Lannon SMCAR-AEE-B, A. Beardell D. Downs S. Einstein S. Westley S. Bernstein J. Rutkowski B. Brodman P. O'Reilly R. Cirincione A. Grabowsky P. Hui J. O'Reilly SMCAR-AEE-WW, M. Mezger J. Pinto D. Wiegand P. Lu C. Hu SMCAR-AES, S. Kaplowitz Picatinny Arsenal, NJ 07806-5000
1	Commander U.S. Army Armament Research, Development and Engineering Center ATTN: SMCAR-HFM, E. Barrieres Picatinny Arsenal, NJ 07806-5000

No. of Copies	Organization
9	Commander U.S. Army Armament Research, Development and Engineering Center ATTN: SMCAR-FSA-T, M. Salsbury SMCAR-FSA-F, LTC R. Riddle SMCAR-FSC, G. Ferdinand SMCAR-FS, T. Gora SMCAR-FS-DH, J. Feneck SMCAR-FSS-A, R. Kopmann B. Machek L. Pinder SMCAR-FSN-N, K. Chung Picatinny Arsenal, NJ 07806-5000
3	Director Benet Weapons Laboratories ATTN: SMCAR-CCB-RA, G.P. O'Hara G.A. Pflegl SMCAR-CCB-S, F. Heiser Watervliet, NY 12189-4050
2	Commander U.S. Army Research Office ATTN: Technical Library D. Mann P.O. Box 12211 Research Triangle Park, NC 27709-2211
1	Director Army Research Office ATTN: AMXRO-MCS, Mr. K. Clark P.O. Box 12211 Research Triangle Park, NC 27709-2211
1	Director Army Research Office ATTN: AMXRO-RT-IP, Library Services P.O. Box 12211 Research Triangle Park, NC 27709-2211
1	Commander, USACECOM R&D Technical Library ATTN: ASQNC-ELC-IS-L-R, Myer Center Fort Monmouth, NJ 07703-5301

No. of Copies	Organization
1	Commandant U.S. Army Aviation School ATTN: Aviation Agency Fort Rucker, AL 36360
1	Program Manager U.S. Tank-Automotive Command ATTN: AMCPM-ABMS, T. Dean Warren, MI 48092-2498
1	Project Manager U.S. Tank-Automotive Command Fighting Vehicle Systems ATTN: SFAE-ASM-BV Warren, MI 48397-5000
1	Project Manager, Abrams Tank System ATTN: SFAE-ASM-AB Warren, MI 48397-5000
1	Director HQ, TRAC RPD ATTN: ATCD-MA Fort Monroe, VA 23651-5143
1	Commander U.S. Army Belvoir Research and Development Center ATTN: STRBE-WC Fort Belvoir, VA 22060-5006
1	Director U.S. Army TRAC-Ft. Lee ATTN: ATRC-L, Mr. Cameron Fort Lee, VA 23801-6140
1	Commandant U.S. Army Command and General Staff College Fort Leavenworth, KS 66027
1	Commandant U.S. Army Special Warfare School ATTN: Rev and Trng Lit Div Fort Bragg, NC 28307
1	Commander Radford Army Ammunition Plant ATTN: SMCAR-QA/HI LIB Radford, VA 24141-0298

No. of Copies	Organization
2	Commandant U.S. Army Field Artillery Center and School ATTN: ATSF-CO-MW, E. Dublisky ATSF-CN, P. Gross Ft. Sill, OK 73503-5600
1	Commandant U.S. Army Armor School ATTN: ATZK-CD-MS, M. Falkovitch Armor Agency Fort Knox, KY 40121-5215
2	Commander Naval Sea Systems Command ATTN: SEA 62R SEA 64 Washington, DC 20362-5101
1	Commander Naval Air Systems Command ATTN: AIR-954-Tech Library Washington, DC 20360
4	Commander Naval Research Laboratory ATTN: Technical Library Code 4410, K. Kailasanate J. Boris E. Oran Washington, DC 20375-5000
1	Office of Naval Research ATTN: Code 473, R.S. Miller 800 N. Quincy Street Arlington, VA 22217-9999
1	Office of Naval Technology ATTN: ONT-213, D. Siegel 800 N. Quincy St. Arlington, VA 22217-5000

No. of Copies	Organization
3	Commander Naval Surface Warfare Center ATTN: Code 730 Code R-13, R. Bernecker H. Sandusky Silver Spring, MD 20903-5000
7	Commander Naval Surface Warfare Center ATTN: T.C. Smith K. Rice S. Mitchell S. Peters J. Consaga C. Gotzmer Technical Library Indian Head, MD 20640-5000
4	Commander Naval Surface Warfare Center ATTN: Code G30, Guns & Munitions Div Code G32, Guns Systems Div Code G33, T. Doran Code E23 Technical Library Dahlgren, VA 22448-5000
5	Commander Naval Air Warfare Center ATTN: Code 388, C.F. Price T. Boggs Code 3895, T. Parr R. Derr Information Science Division China Lake, CA 93555-6001
1	Commanding Officer Naval Underwater Systems Center ATTN: Code 5B331, Technical Library Newport, RI 02840
1	AFOSR/NA ATTN: J. Tishkoff Bolling AFB, D.C. 20332-6448
1	OLAC PL/TSTL ATTN: D. Shiplett Edwards AFB, CA 93523-5000

No. of Copies	Organization
3	AL/LSCF ATTN: J. Levine L. Quinn T. Edwards Edwards AFB, CA 93523-5000
1	WL/MNAA ATTN: B. Simpson Eglin AFB, FL 32542-5434
1	WL/MNME Energetic Materials Branch 2306 Perimeter Rd. STE 9 Eglin AFB, FL 32542-5910
1	WL/MNSH ATTN: R. Drabczuk Eglin AFB, FL 32542-5434
2	NASA Langley Research Center ATTN: M.S. 408, W. Scallion D. Witcofski Hampton, VA 23605
1	Central Intelligence Agency Office of the Central References Dissemination Branch Room GE-47, HQS Washington, DC 20502
1	Central Intelligence Agency ATTN: J. Backofen NHB, Room 5N01 Washington, DC 20505
1	SDIO/TNI ATTN: L.H. Caveny Pentagon Washington, DC 20301-7100
1	SDIO/DA ATTN: E. Gerry Pentagon Washington, DC 21301-7100
2	HQ DNA ATTN: D. Lewis A. Fahey 6801 Telegraph Rd. Alexandria, VA 22310-3398

No. of Copies	Organization
1	Director Sandia National Laboratories Energetic Materials & Fluid Mechanics Department, 1512 ATTN: M. Baer P.O. Box 5800 Albuquerque, NM 87185
1	Director Sandia National Laboratories Combustion Research Facility ATTN: R. Carling Livermore, CA 94551-0469
1	Director Sandia National Laboratories ATTN: 8741, G. A. Beneditti P.O. Box 969 Livermore, CA 94551-0969
2	**Director** **Lawrence Livermore National Laboratory** **ATTN: L-355,** **A. Buckingham** **M. Finger** **P.O. Box 808** **Livermore, CA 94550-0622**
2	Director Los Alamos Scientific Lab ATTN: T3/D. Butler M. Division/B. Craig P.O. Box 1663 Los Alamos, NM 87544
2	Battelle ATTN: TACTEC Library, J.N. Huggins V. Levin 505 King Avenue Columbus, OH 43201-2693
1	Battelle PNL ATTN: Mr. Mark Garnich P.O. Box 999 Richland, WA 99352
1	Institute of Gas Technology ATTN: D. Gidaspow 3424 S. State Street Chicago, IL 60616-3896

No. of Copies	Organization
1	Institute for Advanced Technology **ATTN: T. M. Kiehne** The University of Texas of Austin 4030-2 W. Braker Lane Austin, TX 78759-5329
2	CPIA - JHU ATTN: H. J. Hoffman T. Christian 10630 Little Patuxent Parkway Suite 202 Columbia, MD 21044-3200
1	Brigham Young University Department of Chemical Engineering ATTN: M. Beckstead Provo, UT 84601
1	Jet Propulsion Laboratory California Institute of Technology ATTN: L.D. Strand, MS 125/224 4800 Oak Grove Drive Pasadena, CA 91109
1	California Institute of Technology 204 Karman Lab Main Stop 301-46 ATTN: F.E.C. Culick 1201 E. California Street Pasadena, CA 91109
3	Georgia Institute of Technology School of Aerospace Engineering ATTN: B.T. Zim E. Price W.C. Strahle Atlanta, GA 30332
1	Massachusetts Institute of Technology Department of Mechanical Engineering ATTN: T. Toong 77 Massachusetts Avenue Cambridge, MA 02139-4307
2	University of Illinois Department of Mechanical/Industry Engineering ATTN: H. Krier R. Beddini 144 MEB; 1206 N. Green St. Urbana, IL 61801-2978

No. of Copies	Organization
1	University of Maryland ATTN: Dr. J.D. Anderson College Park, MD 20740
1	University of Massachusetts Department of Mechanical Engineering ATTN: K. Jakus Amherst, MA 01002-0014
1	University of Minnesota Department of Mechanical Engineering ATTN: E. Fletcher Minneapolis, MN 55414-3368
3	Pennsylvania State University Department of Mechanical Engineering ATTN: V. Yang K. Kuo C. Merkle University Park, PA 16802-7501
1	Rensselaer Polytechnic Institute Department of Mathematics Troy, NY 12181
1	Stevens Institute of Technology Davidson Laboratory ATTN: R. McAlevy III Castle Point Station Hoboken, NJ 07030-5907
1	Rutgers University Department of Mechanical and Aerospace Engineering ATTN: S. Temkin University Heights Campus New Brunswick, NJ 08903
1	University of Southern California Mechanical Engineering Department ATTN: 0HE200, M. Gerstein Los Angeles, CA 90089-5199
1	University of Utah Department of Chemical Engineering ATTN: A. Baer Salt Lake City, UT 84112-1194
1	Washington State University Department of Mechanical Engineering ATTN: C.T. Crowe Pullman, WA 99163-5201

No. of Copies	Organization
1	AFELM, The Rand Corporation ATTN: Library D 1700 Main Street Santa Monica, CA 90401-3297
1	Arrow Technology Associates, Inc. ATTN: W. Hathaway P.O. Box 4218 South Burlington, VT 05401-0042
3	AAI Corporation ATTN: J. Hebert J. Frankle D. Cleveland P.O. Box 126 Hunt Valley, MD 21030-0126
2	Alliant Techsystems, Inc. ATTN: R.E. Tompkins J. Kennedy 7225 Northland Dr. Brooklyn Park, MN 55428
1	AVCO Everett Research Laboratory ATTN: D. Stickler 2385 Revere Beach Parkway Everett, MA 02149-5936
1	General Applied Sciences Lab ATTN: J. Erdos 77 Raynor Ave. Ronkonkama, NY 11779-6649
1	General Electric Company Tactical System Department ATTN: J. Mandzy 100 Plastics Ave. Pittsfield, MA 01201-3698
1	IITRI ATTN: M.J. Klein 10 W. 35th Street Chicago, IL 60616-3799
4	Hercules, Inc. Radford Army Ammunition Plant ATTN: L. Gizzi D.A. Worrell W.J. Worrell C. Chandler Radford, VA 24141-0299
2	Hercules, Inc. Allegheny Ballistics Laboratory ATTN: William B. Walkup Thomas F. Farabaugh P.O. Box 210 Rocket Center, WV 26726
1	Hercules, Inc. Aerospace ATTN: R. Cartwright 100 Howard Blvd. Kenville, NJ 07847
1	Hercules, Inc. Hercules Plaza ATTN: B.M. Riggleman Wilmington, DE 19894
1	MBR Research Inc. ATTN: Dr. Moshe Ben-Reuven 601 Ewing St., Suite C-22 Princeton, NJ 08540
1	Olin Corporation Badger Army Ammunition Plant ATTN: F.E. Wolf Baraboo, WI 53913
3	Olin Ordnance ATTN: E.J. Kirschke A.F. Gonzalez D.W. Worthington P.O. Box 222 St. Marks, FL 32355-0222
1	Olin Ordnance ATTN: H.A. McElroy 10101 9th Street, North St. Petersburg, FL 33716
1	Paul Gough Associates, Inc. ATTN: P.S. Gough 1048 South St. Portsmouth, NH 03801-5423
1	Physics International Library ATTN: H. Wayne Wampler P.O. Box 5010 San Leandro, CA 94577-0599

No. of Copies	Organization
2	Princeton Combustion Research Laboratories, Inc. ATTN: N. Mer N.A. Messina Princeton Corporate Plaza 11 Deerpark Dr., Bldg IV, Suite 119 Monmouth Junction, NJ 08852
3	Rockwell International Rocketdyne Division ATTN: BA08, J. Flanagan J. Gray R.B. Edelman 6633 Canoga Avenue Canoga Park, CA 91303-2703
2	Rockwell International Science Center ATTN: Dr. S. Chakravarthy Dr. S. Palaniswamy 1049 Camino Dos Rios P.O. Box 1085 Thousand Oaks, CA 91360
1	Science Applications International Corp. ATTN: M. Palmer 2109 Air Park Rd. Albuquerque, NM 87106
1	Southwest Research Institute ATTN: J.P. Riegel 6220 Culebra Road P.O. Drawer 28510 San Antonio, TX 78228-0510
1	Sverdrup Technology, Inc. ATTN: Dr. John Deur 2001 Aerospace Parkway Brook Park, OH 44142
3	Thiokol Corporation Elkton Division ATTN: R. Willer R. Biddle Tech Library P.O. Box 241 Elkton, MD 21921-0241
1	Veritay Technology, Inc. ATTN: E. Fisher 4845 Millersport Hwy. East Amherst, NY 14501-0305

No. of Copies	Organization
1	Universal Propulsion Company ATTN: H.J. McSpadden 25401 North Central Ave. Phoenix, AZ 85027-7837
1	SRI International Propulsion Sciences Division ATTN: Tech Library 333 Ravenwood Avenue Menlo Park, CA 94025-3493
	Aberdeen Proving Ground
1	Cdr, USACSTA ATTN: STECS-PO/R. Hendricksen

No. of Copies	Organization
1	Ernst-Mach-Institut ATTN: Dr. R. Heiser Haupstrasse 18 Weil am Rheim Germany
1	Defence Research Agency, Military Division ATTN: C. Woodley RARDE Fort Halstead Sevenoaks, Kent, TN14 7BP England
1	School of Mechanical, Materials, and Civil Engineering ATTN: Dr. Bryan Lawton Royal Military College of Science Shrivenham, Swindon, Wiltshire, SN6 8LA England
2	Institut Saint Louis ATTN: Dr. Marc Giraud Dr. Gunther Sheets Postfach 1260 7858 Weail am Rhein 1 Germany
1	Explosive Ordnance Division ATTN: A. Wildegger-Gaissmaier Defence Science and Technology Organisation P.O. Box 1750 Salisbury, South Australia 5108
1	Armaments Division ATTN: Dr. J. Lavigne Defence Research Establishment Valcartier 2459, Pie XI Blvd., North P.O. Box 8800 Courcelette, Quebec G0A 1R0 Canada

INTENTIONALLY LEFT BLANK.

USER EVALUATION SHEET/CHANGE OF ADDRESS

This Laboratory undertakes a continuing effort to improve the quality of the reports it publishes. Your comments/answers to the items/questions below will aid us in our efforts.

1. ARL Report Number ARL-TR-185 Date of Report August 1992

2. Date Report Received _____

3. Does this report satisfy a need? (Comment on purpose, related project, or other area of interest for which the report will be used.) _____

4. Specifically, how is the report being used? (Information source, design data, procedure, source of ideas, etc.) _____

5. Has the information in this report led to any quantitative savings as far as man-hours or dollars saved, operating costs avoided, or efficiencies achieved, etc? If so, please elaborate. _____

6. General Comments. What do you think should be changed to improve future reports? (Indicate changes to organization, technical content, format, etc.) _____

CURRENT ADDRESS

_____
Organization

_____
Name

_____
Street or P.O. Box No.

_____
City, State, Zip Code

7. If indicating a Change of Address or Address Correction, please provide the Current or Correct address above and the Old or Incorrect address below.

OLD ADDRESS

_____
Organization

_____
Name

_____
Street or P.O. Box No.

_____
City, State, Zip Code

(Remove this sheet, fold as indicated, tape closed, and mail.)
(DO NOT STAPLE)

DEPARTMENT OF THE ARMY

OFFICIAL BUSINESS

BUSINESS REPLY MAIL
FIRST CLASS PERMIT No 0001, APG, MD

Postage will be paid by addressee.

Director
U.S. Army Research Laboratory
ATTN: AMSRL-OP-CI-B (Tech Lib)
Aberdeen Proving Ground, MD 21005-5066

NO POSTAGE
NECESSARY
IF MAILED
IN THE
UNITED STATES